Destructive Adsorption of CCl_4 over Lanthanum-Based Solids: Linking Activity to Acid−Base Properties

Alwies W. A. M. van der Heijden,[†] Virginie Bellière,[†] Leticia Espinosa Alonso,[†] Marco Daturi,[‡] Olga V. Manoilova,[†] and Bert M. Weckhuysen*[,†]

Departement Anorganische Chemie en Katalyse, Debye Instituut, Universiteit Utrecht, Sorbonnelaan 16, 354 CA Utrecht, The Netherlands, and Laboratoire Catalyse et Spectrochimie, CNRS, ENSICaen and UCBN, 6, bd Maréchal Juin, 14050 Caen Cedex, France

Received: August 19, 2005; In Final Form: October 24, 2005

The relative activities of a low-surface crystalline and high-surface amorphous LaOCl, further denoted as S1 and S2, have been compared for the destructive adsorption of CCl_4. It was found that the intrinsic activity of S2 is higher than that of S1. Both samples were characterized with X-ray diffraction (XRD), X-ray photoelectron spectroscopy (XPS), N_2-physisorption, and Raman and infrared (IR) spectroscopy. IR was used in combination with CO_2, CO, and methanol as probe molecules. The CO_2 experiments showed that different carbonate species are formed on both materials. For S1, a high surface concentration of bidentate carbonate species and a lower concentration of monodentate carbonate were observed. In the case of S2, bulk carbonates were present together with bridged carbonates. CO adsorption shows that S2 and S1 have very similar Lewis acid sites. However, methanol adsorption experiments showed that S2 had a higher number of stronger Lewis acid sites than S1 and that twofold coordinated methoxy species were more strongly bound than threefold coordinated methoxy species. Because of the analogy between methanol dissociation and the removal of the first chlorine atom in the destructive adsorption of CCl_4, the sites enabling twofold coordination were likely to be the same Lewis acid sites actively involved in the destructive adsorption of CCl_4. La_2O_3 was less active than the two LaOCl materials, and therefore, the intrinsic activity of the catalyst increases as the strength of the Lewis acid sites increases. S2 contains more chlorine at the surface than S1, which is expressed by the higher number of sites enabling twofold coordination. Moreover, this explains the difference in destructive adsorption capacity for CCl_4 that was observed for the samples S1 and S2. Since $LaCl_3$, being the most acidic phase, is not active for the destructive adsorption of CCl_4, basic oxygen atoms, however, remain needed to stabilize the reaction intermediate CCl_3 as La−O−CCl_3.

Introduction

Over the past decades, many chlorinated hydrocarbons (CHC), such as CCl_4, have been banned, and environmentally friendlier alternatives[1] have been introduced. However, because of the increase of the world population, the total amount of CHC consumed is still relatively large. Today, the most commonly used route for CHC destruction is incineration. Even though this process is very efficient[2] (typically > 99%), the high operating temperature makes this a costly method. That is why current research is focusing its attention on finding new effective ways for destroying CHCs at low temperatures and costs.

Potential materials involve alkaline earth metal oxides, lanthanide oxides, and transition metal oxides, and the process of destructive adsorption of chlorinated hydrocarbons has been studied for all these compounds by Klabunde and co-workers[3−8] and several other groups.[9−16] In this reaction, the solid material is chlorinated, while the chlorinated hydrocarbons are oxidized to, e.g., CO_2. In a continuing effort, Van der Avert et al. recently combined the destructive adsorption reaction with a steam dechlorination reaction resulting in a catalytic reaction cycle, which can be envisaged as follows:[17−19]

$$[3CCl_4 + 2M_xO_y \rightarrow 4M_{x/2}Cl_3 + 3CO_{2y/3}] + [4M_{x/2}Cl_3 + 6H_2O \rightarrow 2M_xO_y + 12HCl] = [CCl_4 + 2H_2O \rightarrow CO_2 + 4HCl]$$

The main advantage of this approach is that a continuous process can be constructed, and many materials were tested for their activity in the catalytic destruction of CCl_4 in the presence of steam. The rare earth metal oxides showed the most potential, and from this group, lanthanum oxide possessed the highest destructive capacity. Therefore, our group has studied the lanthanum oxide system in great detail, and it was found that both La_2O_3 and LaOCl are active for the destructive adsorption of CCl_4, although the latter is the most active phase.[21] From previous density functional theory (DFT) calculations, in combination with IR probing experiments, a general trend was observed: surface acidity increases, and conversely, surface basicity decreases in the order La_2O_3 > LaOCl > $LaCl_3$.[20,21] However, a real connection between CHC destruction activity and the acid−base properties of these La-based catalysts is still missing. Therefore, research in our group has concentrated on the physicochemical properties of the LaOCl phase for the conversion of CHCs, such as CCl_4.

The goal of the present contribution is to establish this link between acid−base properties of La-based solids and their destructive adsorption capacity behavior for CCl_4. For this

* To whom correspondence should be addressed. Email: b.m.weckhuysen@chem.uu.nl.
[†] Debye Instituut, Universiteit Utrecht.
[‡] CNRS, ENSICaen and UCBN.

10.1021/jp054689b CCC: $30.25
Published on Web 11/30/2005

purpose, two distinct LaOCl materials have been prepared and characterized in detail, making use of X-ray diffraction, X-ray photoelectron spectrocopy, Raman spectroscopy, and IR spectroscopy, while their acid−base properties were probed with CO, CO_2, and methanol. As a result, it was possible to explain the difference in the reactivity of both solids in terms of difference in Lewis acid strength. This fundamental information provides guidelines for designing new catalyst materials with improved activity for the destruction of CHCs.

Experimental Section

1. Materials. Commercial samples of La_2O_3 (Acros Organics, 99.99%, surface area of 1 m^2/g and pore volume of 0.004 mL/g) and $LaCl_3 \cdot 7H_2O$ (Acros Organics, 99.99%, surface area of 6 m^2/g and pore volume of 0.03 mL/g) were used without additional purification. Two LaOCl materials were synthesized and are further denoted as S1 and S2. S1 was synthesized by a solid-state reaction. An equimolar mixture of La_2O_3 (Acros Organics, 99.99%) and $LaCl_3 \cdot 7H_2O$ (Acros Organics, 99.99%) was exposed to a 20 mL/min flow of O_2 (Hoekloos, 99.995%) at 973 K.[22] S2 was prepared by a precipitation process using $LaCl_3 \cdot 7H_2O$ (Acros Organics, 99.99%) as precursor and an NH_4-OH solution.[23] The obtained gel ($La(OH)_2Cl$) was filtered, washed, and dried at 393 K and calcined at 823 K in pure N_2 for 6 h.

2. Characterization. The phase purity of the La-based materials was checked with X-ray diffraction (XRD). XRD measurements were collected for both samples at ambient conditions with a Bruker-Nonius PDS 120 powder diffractometer system, equipped with a position-sensitive gas-filled detector of 120° 2θ, using Co Kα_1 radiation ($\lambda = 1.788\,97$). A Phillips XL-30 field emission gun (FEG) scanning electron microscope was used to obtain the SEM images. X-ray photoelectron (XPS) spectra were acquired using a Perkin-Elmer (PHI) model 5500 spectrometer. All spectra were obtained using samples in the form of pressed wafers. XPS data were obtained for S1 and S2, both before and after reaction with CCl_4. Raman spectra were recorded with a Holoprobe Kaiser Optical spectrometer equipped with a holographic notch filter, CCD camera, and 532 nm laser. All spectra were measured under ambient conditions. The specific surface area and pore volume have been determined by N_2 sorption measurements with a Micromeritics accelerated surface area and porosimetry ASAP 2400 instrument. Surface areas were calculated by using the BET model with micro- and macropores described by the Horvath−Kawazoe and BJH models, respectively. IR spectra were collected using a Nicolet 550 spectrometer with a resolution of 4 cm^{-1}. A glass cell was used at room temperature. The samples, about 20 mg for S2 and 30 mg for S1, were pressed into self-supported 2 cm^2 disks and activated in situ prior to IR measurements. Both S1 and S2 were pretreated in a vacuum ($\sim 10^{-4}$ Pa) at 820 K. Methanol (Sigma-Aldrich, 99.9+ %) was initially dosed to an equilibrium pressure of 1.3 mbar. The gas was then progressively evacuated at room temperature and then at increasing temperatures up to 473 K. CO_2 (Air Liquide, Inc., 99.99+ %) was dosed in steps to equilibrium pressures up to 6.5 mbar. For CO sorption, a stainless steel IR cell was equipped with crystalline ZnSe inner windows, which, in combination with the outer KBr windows, allowed it to collect spectra in the region of 4000−500 cm^{-1} at 77−300 K.

The samples were pressed into self-supported 2 cm^2 wafers and activated in situ prior to IR measurements in a vacuum at 820 K for 2−3 h. Before adsorbate introduction, the samples were cooled to the corresponding experimental temperatures (77 K) under a vacuum of $5 \cdot 10^{-5}$ mbar. It is important to note that the cell should be cooled below 270 K, keeping the sample in the upper part of the cell to prevent the humidity absorbed on the cell walls to reach the sample surface. CO was dosed at 77 K to ~6 mbar equilibrium pressure of CO and progressively desorbed in a closed cell by raising the temperature in the range 77−210 K. In this case, the pressure inside the cell rose to 10−12 mbar because of desorption and cell heating. The low-temperature IR spectra were recorded using a Bruker IFS166 spectrometer with 3 cm^{-1} spectral resolution. Temperature-programmed desorption (TPD) experiments with CO_2 were performed on S1 and S2 in a tubular reactor under He flow with the effluent analyzed by a Micromeritics Autochem II chemisorption analyzer. The heating rate was 5 K/min. Atmospheric CO_2 was adsorbed on samples S1 and S2 after long-term exposure to air at ambient conditions. No pretreatment was used for these experiments.

3. Activity. The activity measurements for the destructive adsorption of CCl_4 were performed in a tubular fixed-bed quartz reactor. The catalyst bed consisted of 1.0 g of sample pressed in a 150−500 μm sieve fraction, pretreated in a 10 mL/min He flow at 823 K. In the case of La_2O_3, the pretreatment was under O_2 flow instead of He. The flow was regulated by Brooks 0−100 mL automatic mass flow controllers. To find the initial reaction temperature, the reaction was carried out from 323 to 673 K using a 20 mL/min 6 vol % CCl_4/He flow. This flow was generated by bubbling He through a bubbler containing CCl_4 for 30 min out through a vent. Once stabilized, the flow was led over the reactor bed, consisting of La_2O_3, S1, S2, and $LaCl_3$, respectively. The temperature of the reactor was raised from 323 to 673 K in steps of 10 K. The heating ramp was 3 K/min, and after each step of 10 K, the temperature was held constant for 5 min. The composition of the reactor effluent was analyzed by a Siemens Maxum Edition 2 gas chromatograph with a sampling time of 5 min. In the case of S1 and S2, the reactions were also performed at a constant temperature of 473 K. The flow was stabilized as described above and led over the pretreated reactor bed at 473 K. The composition of the reaction mixture was analyzed with time.

Results and Discussion

1. Materials Synthesis and Characterization. Table 1 summarizes the physicochemical properties of the La-based materials under study. The N_2 sorption results show that S2 has a relatively large surface area and pore volume. La_2O_3 possesses a very low surface area and pore volume, but has a larger average pore size than S1 and S2. S2 shows a more open structure compared to S1 and La_2O_3. More importantly, the high surface area means that there will be more reaction sites available for S2 than for S1. The XRD patterns of S1 and S2 are shown in Figure 1 and resemble those of tetragonal LaOCl.[24] As a reference, the diffractogram of La_2O_3 is also shown in Figure 1, and the XRD peak positions and intensities for LaOCl,[24] $LaCl_3$,[25] and $La_2O(CO_3)_2$[26] are shown in Table 2. However, both the reflection intensities and the background level clearly vary with the preparation method. Intense and sharp reflection peaks associated with a very weak background are observed for S1, pointing out the high crystallinity of this sample. In contrast, the XRD patterns of S2 features broad reflections of very low intensity compared to S1, while the background level is particularly high. This indicates that S2 contains a small number of LaOCl crystallites embedded in an amorphous phase. Also, additional peaks are present in the XRD

TABLE 1: Physicochemical Properties of the La-Based Catalyst Materials under Study, Together with the Phase Purity as Determined with XRD and Raman (na = not applicable)

sample name	surface area (m^2/g)	pore volume (mL/g)	average pore size (nm)	as determined with XPS		phases as determined with Raman	phases as determined with XRD
				O/La	O/Cl		
La_2O_3	1	0.001	14.3	0.34	na	La_2O_3	La_2O_3 La carbonates
S1	6	0.040	23.6	0.17	2.78	LaOCl	LaOCl
S2	36	0.300	34.0	0.14	1.80	LaOCl	LaOCl $LaCl_3$ La carbonates
$LaCl_3$	6	0.030	22.4	na	na	$LaCl_3$	$LaCl_3$

of S2. When compared to reference materials,[25,26] a large amount of $La_2O(CO_3)_2$ was found to be present in S2. The lanthanum carbonates are most likely formed with CO_2 from the water or the air during precipitation. The carbonates are very stable and remain in the material up to a temperature of 1000 K.[21]

Scanning electron microscopy (SEM) photographs of S1 and S2 are presented, respectively, in Figure 2A,B. S1 material shows a very homogeneous distribution of polycrystallites with lengths centered on ca. 4 μm and thicknesses of <1 μm. This particular shape of the grains reflects well the layered crystalline structure of LaOCl. The SEM picture of S2 sample shows polycrystallites of small size having a rodlike shape. The difference in morphology observed in the XRD results is therefore confirmed by these SEM images.

The Raman spectra presented in Figure 3 both show that the main phase of S1 and S2 is LaOCl, as evidenced by the bands at 331 and 437 cm^{-1}.[4] Especially, the Raman spectrum of S2 shows other bands at 413, 363, 301, and 243 cm^{-1}. No reference was found with respect to these bands, but they possibly result from bulk lanthanum carbonate. However, the Raman band indicative of carbonates around 1000 cm^{-1} is not observed in the spectrum, and it is presently unclear why these differences occur between XRD and Raman. The bands at 413, 363, 301, and 243 cm^{-1} may therefore result from the background and have become visible because of the low intensity of the LaOCl bands. XPS also provides information regarding the phase purity of S1 and S2. According to Table 1, the O/La surface ratio for La_2O_3 is 0.34 and for $LaCl_3$ is 0. For S1, the value of 0.17 again shows that it is a very pure LaOCl phase. S2 has a slightly lower O/La ratio and should therefore be more chlorinated.

2. Materials Acid−Base Properties. *2.1. CO_2 Adsorption.* CO_2 was adsorbed to probe the basicity of the materials under study. CO_2 can act as a Lewis acid toward either O^{2-} surface ions resulting in the formation of carbonate species or residual basic OH surface species resulting in the formation of hydrogen carbonates. Furthermore, CO_2 can act as a Lewis base and form carboxylates. The possible compounds resulting from CO_2 coordination are described in Scheme 1.[27] For the carbonates, the principal anchoring structures are included in this scheme. The IR spectra after CO_2 adsorption are shown in Figure 4. The spectra were obtained by subtraction of the spectrum measured directly after pretreatment. In all spectra, the spectrum of gas-phase CO_2 was subtracted in order to display only the surface species. The spectra were also normalized for the amount of sample and the surface area. The band at 1450 cm^{-1} in the spectrum of S2 appeared as a result of the subtraction.

For S1, three main bands were observed at 1589, 1423, and 1266 cm^{-1}. Smaller bands were present at 2349, 1523, 1326, and 1200 cm^{-1}. Bands, which are not shown here, were also detected at 1036, 845, 826, 729, 708, and 669 cm^{-1}. The latter is a bending mode of molecular CO_2. The band at 2349 cm^{-1} was only observed at high equilibrium pressures. This band is

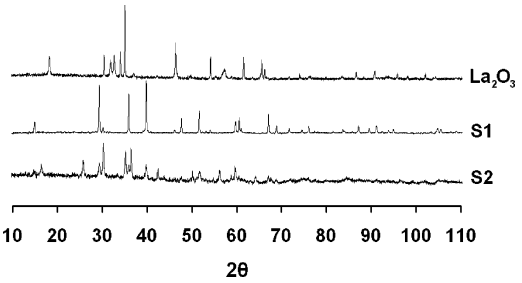

Figure 1. X-ray diffractogram of La_2O_3, S1, and S2 materials measured under ambient conditions.

TABLE 2: XRD Positions and Relative Intensities for $LaCl_3$, LaOCl, and $La_2O(CO_3)_2$

LaOCl		$LaCl_3$		$La_2O(CO_3)_2$	
2θ (°)	relative intensity	2θ (°)	relative intensity	2θ (°)	relative intensity
25.9	326	15.9	999	14.9	400
29.3	290	27.7	315	29.3	1000
30.0	747	28.6	520	35.8	1000
35.4	999	32.1	141	39.6	750
39.3	229	36.7	221	47.5	500
52.0	487	40.3	719	51.4	950
55.8	359	42.9	128	59.6	350
59.2	214	48.2	152	60.4	900
67	227	48.9	240	67.0	850
		49.4	508	75.6	750
		71.0	130	86.9	500

generated by the coordination of CO_2 on Lewis acid sites of the surface. The main band at 1423 cm^{-1} has been attributed to the doubly degenerated asymmetric ν_3 stretch of the free carbonate ion. In the present case, it corresponds to a polydentate carbonate, having a strong ionic character. In the adsorbed state, the symmetry of the carbonate ion is lowered, and the species generally present two split ν(CO) bands at either side of the band at 1423 cm^{-1}.[28] This is the case for the other two main bands at 1589 and 1266 cm^{-1}, which are both at 166 cm^{-1} from this band. The bands at 1523 and 1326 cm^{-1} are also coupled with a $\Delta\nu_3 = 100$ cm^{-1}, where $\Delta\nu_3$ is the difference in frequency between the ν_3 stretch of the free carbonate ion and the split bands. It has been shown that bidentate carbonate species generally present a $\Delta\nu_3$ split between 150 and 300 cm^{-1}, and bridging carbonate species have a $\Delta\nu_3$ split above 300 cm^{-1}.[28] The bands with $\Delta\nu_3 = 100$ cm^{-1} are indicative of either monodentate or polydentate carbonates. Using these considerations, we can unfortunately not distinguish between monodentate and polydentate carbonates, except for their thermal stability, with the former being less stable at higher temperature. The relative intensities of the bands in the spectrum of S1 would then be attributed to a low concentration of monodentate or polydentate carbonates and a high concentration of bidentate carbonate. Also, the band at 845 cm^{-1} is attributed to the π-(CO_3) of bidentate carbonate,[28] and the band at 1036 cm^{-1} has

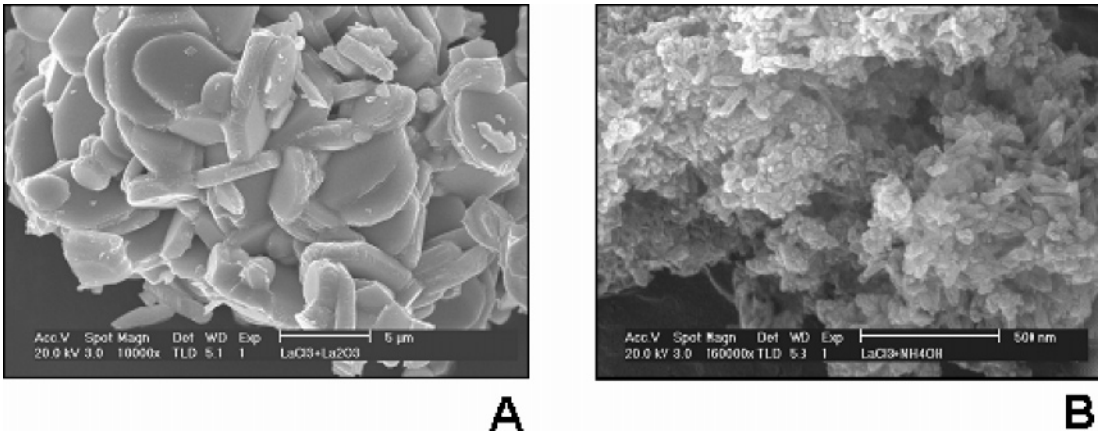

Figure 2. Scanning electron micrographs of (A) S1 and (B) S2 materials.

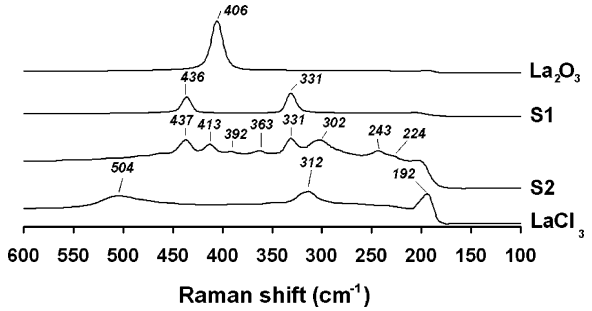

Figure 3. Raman spectra of La_2O_3, S1, S2, and $LaCl_3$ materials measured under ambient conditions.

SCHEME 1: Possible Surface Structures as a Result of CO_2 Adsorption on Lanthanum Oxide

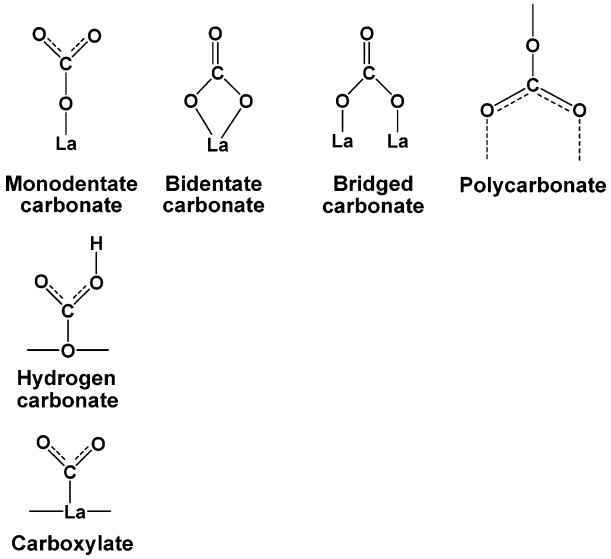

been attributed to the symmetric C−O stretching of bidentate carbonate.[29] The presence of a weak, but sharp, band at 1201 cm^{-1} could be indicative of the presence of hydrogen carbonates (δ(OH) mode).[28] In such a case, the corresponding stretching modes will be found at around 1600 cm^{-1} (a shoulder in the high-wavenumber tail of the bidentate carbonate band) and below the 1266 cm^{-1} peak. The corresponding ν(OH) mode could be guessed at around 3624 cm^{-1}, but that region is however very noisy. If confirmed, the presence of hydrogen carbonate species will be indicative of the basicity of hydroxyl groups.

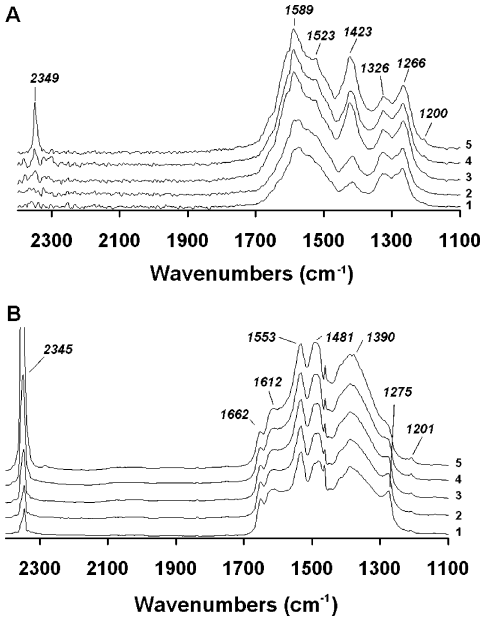

Figure 4. FTIR spectra of adsorbed CO_2 on (A) S1 and (B) S2 after 15 min of equilibration at CO_2 pressures of (1) 0.05, (2) 0.1, (3) 0.3, (4) 1.3, and (5) 6.5 mbar.

In the spectra of S2, the band of weakly adsorbed CO_2 is also present, but the band is present in all spectra and not just at a high equilibrium pressure. This indicates that these species are more strongly adsorbed and that the Lewis sites are more acidic. In fact, the band is also slightly shifted to lower wavenumbers. The IR spectra are very different from those of S1 in the carbonate region. A broad set of bonds is present even at low equilibrium pressure. A similar spectrum was obtained for CO_2 adsorption on La_2O_3 as reported by Manoilova et al.[21] Also, the IR spectrum of $La_2(CO_3)_3$ is characterized by these adsorption bands between 1650 and 1250 cm^{-1} with two peaks at 1483 and 1390 cm^{-1}.[30] The bands at 1662, 1612, and 1278 cm^{-1} were also observed by Manoilova et al. in the spectra of LaOCl and were attributed to bridged carbonate. In that case, however, these bands appeared simultaneously with another band due to bridged species on two different O adsorption sites. In the case of S2, they are not coupled, indicating that the two O adsorption sites of these bridged species are not different. Another interpretation is that the band at 1612 cm^{-1} would be assigned to hydrogen carbonates, which are confirmed for S2 by the modes at 1208 and 3624 cm^{-1}. So, only the bands at 1652 and 1275 cm^{-1} are likely to be assigned to a single species

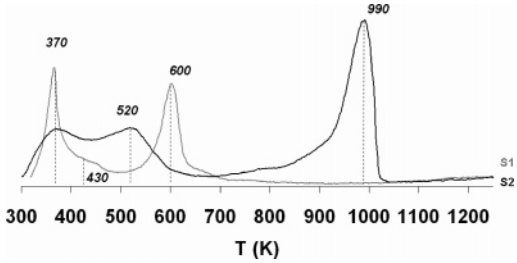

Figure 5. TPD of CO_2 adsorbed from the air under ambient conditions on LaOCl material: S1 (gray) and S2 (black).

TABLE 3: Desorption Temperatures for La-Based Reference Compounds

reference compound	structure	desorption temperature (K)
La_2O_3	$La_2(CO_3)_3 \rightarrow La_2O_3{\cdot}xCO_2 + (3-x)CO_2$ (g)	570−675
	$La_2O_3{\cdot}xCO_2 \rightarrow La_2O_3 + xCO_2$ (g)	770−1000
LaOCl	physisorbed $CO_2 \rightarrow CO_2$ (g)	370
	bridged carbonates → polydentate carbonates + CO_2 (g)	563
	polydentate carbonates → CO_2 (g)	894
$LaCl_3$	physisorbed $CO_2 \rightarrow CO_2$ (g)	370
CeO_2	monodentate → CO_2 (g)	300
	bidentate → CO_2 (g)	500

of bridged carbonates. Previously, the IR frequencies for mondentate, bridged, and polydentate carbonates have been calculated by DFT,[20] but the geometries for the bridged type tended to converge into the polydentate structure. This may explain the observed difference between the calculated [20] and experimentally observed frequencies.

2.2. Temperature-Programmed Desorption. To discriminate between the presence of either polycarbonate or monodentate carbonate on S1, a temperature-programmed desorption (TPD) with CO_2 was performed. Similar experiments were also done for S2 to verify the type of carbonates detected on the surface. The results are given in Figure 5. In Table 3, reference compounds and their respective desorption temperatures are tabulated.[21,23]

For S1, the first signal on the thermal conductivity detector (TCD) is measured at 300−450 K. At this temperature, water is desorbed from the surface. A small shoulder is also present around 430 K, which has been assigned to physisorbed CO_2. Another peak becomes visible at 510−700 K, which also possesses a low-intensity shoulder. The main band can be assigned to either bidentate or bridged carbonate species. However, in the case of bridged species, polydentate carbonates would be formed as a result of the CO_2 desorption. Since no signal is detected above 750 K and polydentate carbonates desorb around 894 K, the signal is most likely indicative of bidentate carbonates. No references were found regarding the low-intensity shoulder at 670 K. IR spectroscopy was unable to discriminate between polydentate carbonates and monodentate carbonates before, but as stated above, no polydentate carbonates were detected by TPD. The band for monodentate carbonates is usually measured around 300 K but is hard to distinguish, since physisorbed CO_2 and water also desorb in this region. However, according to the IR results, monodentate carbonates are formed upon adsorption of CO_2 on S1. Therefore, on S1, a low concentration of monodentate species and a high concentration of bidentate carbonates is expected to be present after adsorption of CO_2.

For S2, two TCD peaks are visible in the region between 300 and 650 K. One possesses a maximum at 350 K and the other at 500 K. As for sample S1, the former is assigned to water and physisorbed CO_2, while the latter is indicative of either bidentate or bridged carbonate species. Another option is the decomposition of bulk carbonates. A peak between 770 and 1000 K would then also be visible, and this is in fact the case. In the case of bridged species, formation of polydentate carbonates would be the result of CO_2 desorption. IR results indicated the presence of bridged carbonates and bulk carbonates. This is certainly a possibility, but the TPD results cannot discriminate between bridged carbonates and bulk carbonates, since they possess desorption peaks in the same temperature regions. On the basis of both the IR results and the TPD results, the formation of bridged and bulk carbonates takes place upon adsorption of CO_2 on S2.

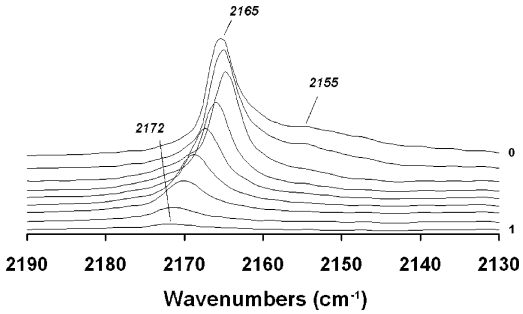

Figure 6. FTIR spectra of CO adsorbed on S1 at 6 mbar equilibrium pressure (spectrum 0) and consecutive desorption of CO, while the temperature is increased from 77 to 210 K (spectrum 1) for the region of CO coordinated on Lewis acid sites.

2.3. CO Adsorption. CO adsorption can be used to probe Lewis acidity. Absorption bands located at high wavenumbers are related to strong M−CO bonds, which is a consequence of a strong Lewis acid site. On the basis of IR spectra during adsorption and desorption of CO, a distribution of the strengths of the Lewis acid sites can be obtained.

Figure 6 shows the IR spectra for sample S1 obtained after CO adsorption and consecutive desorption for increasing measurement temperature. Because of the low surface area and relatively high activation temperature, no IR bands due to hydroxyl groups could be discovered. As a consequence, we concentrate our analysis on the ν(CO) region. After CO adsorption at 77 K, a strong band at 2165 cm^{-1} was observed with a weak shoulder at 2155 cm^{-1}, likely witnessing the presence of Brønsted acid sites. After CO desorption, the band at 2155 cm^{-1} disappears quickly, and the band at 2165 cm^{-1} decreases in intensity and shifts to 2172 cm^{-1}. The CO adsorption band and the consecutive desorption of CO show the distribution in strength of the Lewis acid sites at the surface of S1. The strongest Lewis acid sites on S1 are therefore represented by the band that remains after CO desorption at 2172 cm^{-1}.

In the IR spectrum of S2 presented in Figure 7, a weak band of the hydroxyl groups was observed at 3650 cm^{-1}, so confirming the presence of small amounts of Brønsted acid sites. After CO adsorption at 77 K, the free OH band disappeared completely, and a perturbed one becomes visible at 3615 cm^{-1}. In the CO region of the IR spectra, the strong band at 2165 cm^{-1} and a weak and broad one at 2155 cm^{-1} were observed. After CO desorption, the band at 2155 cm^{-1} decreases in intensity. At the same time, a free hydroxyl band reappears, and the perturbed one at 3615 cm^{-1} diminishes. In other words, the band at 2155 cm^{-1} can be assigned to H-bonded CO. After CO desorption, the band at 2165 cm^{-1} shifts toward higher wavenumber at 2171 cm^{-1}. As with S1, the distribution of the

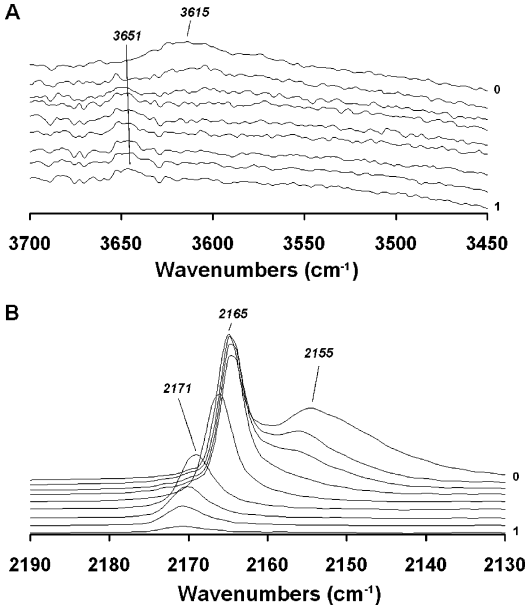

Figure 7. FTIR spectra of CO adsorbed on S2 at 6 mbar equilibrium pressure and consecutive desorption of CO, while the temperature is increased from 77 to 210 K for (A) the region of OH vibrations and (B) the region of CO coordinated on Lewis acid sites.

SCHEME 2: Types of Irreversibly Adsorbed Alcohols on Metal Oxides

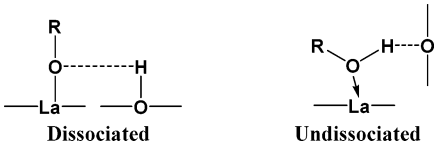

strengths of the Lewis acid sites is reflected in the spectra upon desorption. In the case of S2, the strongest Lewis acid site is represented by the band at 2171 cm^{-1}. So, S1 and S2 have identical Lewis acid sites and also show no large differences in the distribution of the Lewis acid sites. Thus, the type of sites available on samples S1 and S2 cannot be distinguished by CO adsorption using IR spectroscopy. To discriminate between the different sites, another more powerful probe molecule is needed. In our opinion, this is methanol.

2.4. CH_3OH Adsorption. Two types of irreversibly adsorbed species (species which are not removed by a relatively short evacuation at room temperature) can be formed on adsorption of alcohols on metal oxides: alkoxy species, resulting from dissociative chemisorption on a very weak Lewis acid site located near a very basic one, and undissociated species, coordinated on a strong Lewis acid site.[31] This is schematically represented in Scheme 2. Adsorption of methanol is, however, much less specific, since it could also occur on couples having a predominantly Lewis acid character. The respective dissociation processes of an acid/base couple with predominant Lewis acid and base character can be envisaged as in Scheme 3.[19] Dissociation of methanol on an acid−base couple is similar to the first reaction step for the destruction of CCl_4. DFT calculations have shown that CCl_4 is split into two fragments: $Cl^{\delta-}$, coordinated toward the Lewis acid site, and $CCl_3^{\delta+}$, stabilized on the basic oxygen.[20] Methanol is also split into two fragments: methoxy species coordinated toward the Lewis acid site and a hydrogen atom, which is transferred to the basic oxygen site. Since the same acid−base couple is needed for both processes, the methanol adsorption results are very likely to give information on the active site for the destructive

SCHEME 3: Dissociation Process of Methanol on an Acid/Base Couple with Predominant (A) Lewis Acid and (B) Lewis Base Character

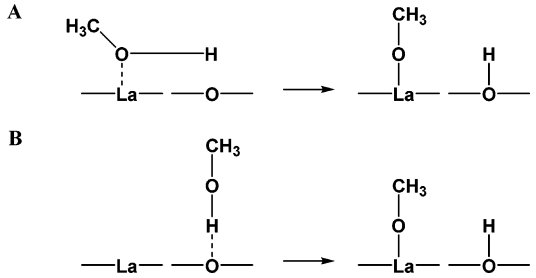

SCHEME 4: Dissociation Process of (A) Methanol and (B) CCl_4 on an Acid/Base Couple

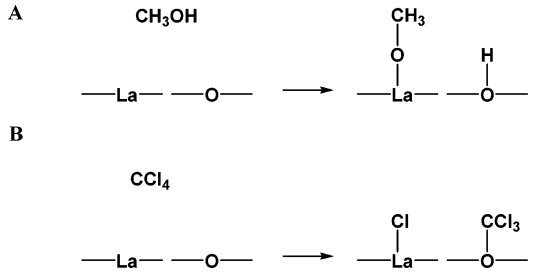

adsorption of CCl_4 over La-based materials as well. The comparison between CCl_4 and methanol dissociation on a La−O acid−base couple is shown in Scheme 4. Because, compared to oxygen, the chlorine atom is more electronegative, the La−Cl bond formed during the dissociation is stronger than the La−OCH_3 bond, and the Cl is more difficult to desorb.

The IR results of the adsorption of methanol on S1 and S2 are shown in Figure 8. For the spectra at 1.3 mbar of methanol in equilibrium at room temperature (RT), the spectrum of gas-phase methanol was subtracted. The spectra were also normalized for the amount of sample and the surface area. The IR spectrum of S1 at equilibrium shows a main band at 1033 cm^{-1}. This band was also visible in the gas-phase spectrum of methanol and is attributed to physisorbed species. A small band is present at 1104 cm^{-1}, which is attributed to an on-top coordinated methoxy species on a La^{3+} site.[32] After 15 min of evacuation at RT, the weakly adsorbed species have been removed. Also, the band of linearly adsorbed methoxy species has decreased in intensity, and two small bands have become better resolved at 1062 and 1012 cm^{-1}. These bands are attributed to doubly bridged and threefold coordinated methoxy species, respectively.[32] Upon further evacuation, these bands also disappear, and a band becomes visible at 1043 cm^{-1}, which is also caused by the twofold coordination of adsorbed methoxy species.[32] It has been proposed that the two bridging species are differing from the coordinative unsaturation of the cations constituting the site.[32] The possible coordinated methoxy species can be envisaged as in Scheme 5. As with S1, a strong band resulting from a weakly adsorbed species is visible on S2 at 1033 cm^{-1}, which is removed by evacuation at RT. Again, bands become visible after evacuation at RT at 1017, 1062, and 1101 cm^{-1}, attributed to threefold coordinated, doubly bridged, and linearly adsorbed methoxy species, respectively. The bands of threefold coordinated and linearly adsorbed methoxy species have disappeared after evacuation at 373 K. After evacuation at 423 and 473 K, the broad bands of the doubly bridged species show a different behavior for its two components, with the doubly bridged species in the presence of defects (those at lower wavenumbers) being less susceptible to evacuation. It seems

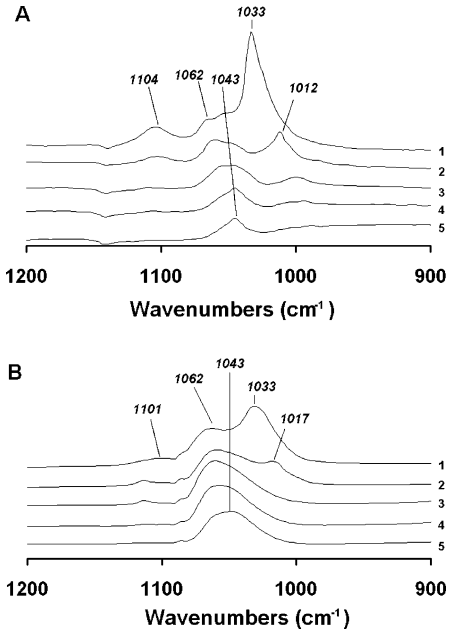

Figure 8. FTIR spectra of methanol adsorbed on (A) S1 and (B) S2 at (1) 1.3 mbar equilibrium pressure and the consecutive desorption by (2) evacuation at RT, (3) evacuation at 373 K, (4) evacuation at 423 K, and (5) evacuation at 473 K.

SCHEME 5: Possible Coordinated Methoxy Species to La-Based Materials

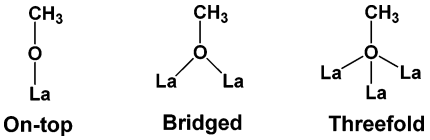

that at higher loading the methoxy species prefer a doubly bridged coordination, where at lower loading threefold coordination is preferred. Also, the methoxy species remain adsorbed at much higher temperatures than on S1, which indicates the presence of relatively more acidic Lewis sites on S2. To verify this hypothesis, we have integrated the area under the adsorption bands for the adsorbed methoxy groups. The results are summarized in Table 4. The integrated area is normalized for the surface area.

It is clear that the integrated area is larger for S1 for spectra 1, 2, and 3. These spectra are, however, dominated by the physisorbed methanol and the weakly adsorbed methoxy species, such as the threefold and linearly adsorbed species. The bridged methoxy species are adsorbed more strongly and remain on the surface the longest. In spectra 4 and 5, the bridged methoxy species are the only species remaining on the surface of S1 and S2. In these spectra, however, S2 has a larger integrated area than S1. This indicates that S1 might contain more Lewis acid sites, but S2 possesses the strongest Lewis acid sites. The difference between S1 and S2 was the amount of chlorine present at the surface, as was determined by XPS. Apparently, the higher amount of chlorine is not reflected in the strength of the Lewis acid sites, but in the number of specific sites that are present. For S2, the sites to which the methoxy species were most strongly adsorbed, namely, the sites forming bridged methoxy species, are more abundant than for S1.

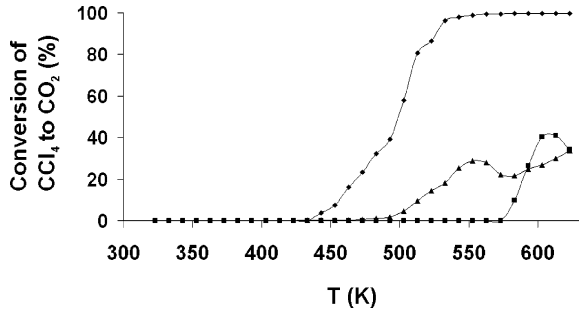

Figure 9. Conversion of CCl_4 to CO_2 on La_2O_3 (■), S1 (▲), and S2 (◆) materials measured as a function of temperature.

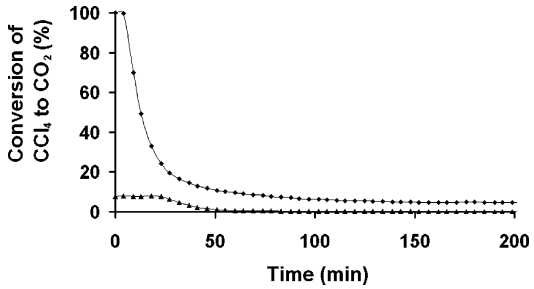

Figure 10. Conversion of CCl_4 to CO_2 measured at 473 K for samples S1 (▲) and S2 (◆).

3. Activity Measurements. In a first series of experiments, we have studied the destructive adsorption of CCl_4 over La_2O_3, S1, and S2 as a function of the reaction temperature, and Figure 9 shows the conversion of CCl_4 to CO_2 for these three materials. The first CO_2 is detected at 573 K for La_2O_3, and a sharp increase in the amount of CO_2 is observed at higher temperatures. The formation of carbonates might delay the detection of CO_2; however in previous TPD measurements,[21] CO_2 was already released at 500 K from La_2O_3 which contained carbonates. Since, during the experiment, CO_2 is not detected until 573 K, the interference of carbonate formation with our experiments is not likely. For S1 and S2, no phosgene is formed during the experiment. The initial reaction temperature is for both oxychlorides at 443 K. This is at a much lower temperature than for La_2O_3, which means that both oxychloride materials are more active than La_2O_3. Since the samples become chlorinated during the reaction, the initial temperature of reaction is the only information available from these measurements.

To be able to compare S1 and S2, the materials were tested for the CCl_4 destruction reaction at constant temperature of 473 K as well. The results are shown in Figure 10. The activity curves of the two LaOCl can be divided into four areas. In the first part of the measurement, the conversion is constant and controlled by the transformation of CCl_4 into the products. It should be noted that for S2 the conversion is 100% in the first area of the curve. Therefore, even though not visible, the

TABLE 4: Relative Integrated Areas under Spectra of Figure 8 at Different Stages of Methanol Adsorption/Desorption on Samples S1 and S2

conditions	species present	S1	S2
methanol at equilibrium pressure of 1.3 mbar	physisorbed methanol linear, bridged, and threefold methoxy species	17.2	6.0
evacuation at room temperature	linear, bridged, and threefold methoxy species	7.6	4.1
evacuation at 373 K	bridged and threefold methoxy species	4.3	3.6
evacuation at 423 K	bridged and threefold methoxy species	2.8	3.1
evacuation at 473 K	bridged methoxy species	1.8	2.5

TABLE 5: XPS Results of Sample S1 Before and After Reaction with CCl_4 at Various Temperatures

sample	O/La	O/Cl
before reaction	0.17	2.8
after reaction at 473 K	0.19	1.7
after reaction at 483 K	0.21	1.6
after reaction at 493 K	0.18	1.4

conversion may have decreased in the beginning of the reaction. Then, as the rate of conversion decreases, bulk diffusion limitations take effect. After this, the conversion stabilizes and reaches a steady state, where the reaction is controlled by diffusion of oxygen to the surface and chlorine to the bulk. Finally, the material becomes deactivated, and the conversion drops to almost zero. After reaction at constant temperature, resulting in deactivation, XPS and Raman were performed on the deactivated S1 sample. S2 was not measured in this way, since it took very long to deactivate.

The Raman spectra before and after reaction did not show any change in band positions or intensity. Apparently, no change in the bulk phase was observed as a result of the reaction. The XPS results tabulated in Table 5 show a decrease in oxygen and an increase of chlorine at the surface. Even though S1 has become deactivated, oxygen is still present at the surface. The final chlorine content increases with the temperature of reaction. Higher temperatures result in a prolonged O/Cl bulk/surface diffusion. Bulk diffusion decreases as the chlorine content increases. However, an increased temperature facilitates O/Cl diffusion, allowing diffusion to continue even at higher chlorine content.

S2 has a much higher destruction activity, which was expected in view of the high surface area of S2. Therefore, the conversion has to be normalized to enable a fair comparison between the activities of S1 and S2. The conversion, 8% for S1 and 100% for S2, is therefore divided by the surface area to get the activity per square meter of material. During the reaction, the surface area that was calculated with N_2 physisorption changes as a result of the chlorination. For the first area of the curves, the change in surface area is assumed not to be significant. For S1 and S2, respectively, the destructive capacities were $4.2 \cdot 10^{-7}$ and $8.7 \cdot 10^{-7}$ mol CO_2 formed per square meter of material per minute. However, for S2, the obtained destructive adsorption is a lower limit. So, after normalization, S2 is twice as active as S1. The key factor in the activity is the strength of the acid−base couple responsible for the reaction.[5] The Lewis acid site initiates the reaction by splitting off a chlorine atom. Therefore, the trend in activity, $La_2O_3 < S1 < S2$, parallels the trend in surface acidity. However, $LaCl_3$ is not active for the destructive adsorption of CCl_4, even though it is more acidic than the other materials. This is because of the absence of basic oxygen sites, which stabilize the CCl_3 fragment remaining after the initial split of a chlorine atom by the acid site. Moreover, the absence of oxygen simply implies that no stoichometric reagent is available for CO_2 formation.

In summary, the two main parameters determining the overall activity are the strength of the Lewis acid site and the availability of basic oxygen sites next to the acid site to stabilize the reaction intermediate CCl_3. The increased chlorine content results in a stronger acid site, but this also decreases the number of oxygen sites. An optimum value of activity is therefore to be expected for a phase with a chlorine content lower than $LaCl_3$ but higher than that of pure LaOCl. Moreover, the reaction becomes diffusion-limited after prolonged reaction with CCl_4. The addition of the right amount of steam seems therefore to be crucial to ensure the presence of the optimal catalyst phase composition during the catalytic destruction of CCl_4.

Conclusions

The following conclusions can be drawn from this work:

1. The synthesis method has a dramatic influence on the bulk as well as on the surface properties of LaOCl materials. S1, prepared via a solid-state reaction, is highly crystalline and a pure LaOCl phase. The high crystallinity is also reflected by its low surface area and pore volume. S2, prepared via a sol/gel reaction, is characterized by a relatively high surface area and pore volume. S2 mainly consists of LaOCl crystallites embedded in an amorphous phase. Moreover, S2 contains bulk lanthanum carbonate.

2. IR spectroscopy, in combination with probe molecules such as CO_2, CO, and methanol, is a powerful method to assess the acid−base properties of LaOCl materials. Lewis acidity has been probed with CO and methanol. The CO adsorption has shown that S1 and S2 do possess similar Lewis acid sites. On the other hand, methanol probing shows that S2 contains a larger number of strong adsorption sites than S1, more specifically sites that are likely used for the destructive adsorption of CCl_4. The larger amount of chlorine at the surface that was observed with XPS appears to increase the number of active Lewis acid sites at the surface of S2. Basicity has been assessed via CO_2 adsorption, and these experiments show that the type of carbonate formed on S1 and S2 differs. In the case of S1, a high amount of bidentate carbonates and a low amount of monodentate carbonates are observed. For S2, however, bulk carbonates are formed together with some bridged carbonates.

3. La-based materials are active in the destructive adsorption of CCl_4, and the following activity trend was observed: $LaCl_3 \ll La_2O_3 < S1 < S2$. The difference in Lewis acidity between La_2O_3 and LaOCl is reflected by the lower initial reaction temperature of LaOCl. The higher activity of S2 is caused by the higher density of active Lewis acid sites on S2 in comparison with S1. These two conclusions are combined by the observation with XPS that, for the oxygen-rich surfaces of S1 and S2, S2 contains more chlorine. Because chlorine is more electronegative than oxygen, more strong Lewis acid sites are available on S2. However, these differences in strength cannot be revealed by CO IR adsorption measurements. Nevertheless, we believe that the strength of a Lewis acid site remains a key factor for activity and a stronger Lewis acid site results in higher intrinsic activity for CCl_4 destruction. However, basic oxygen sites remain necessary to enable the conversion of CCl_4 to CO_2. In other words, the appropriate acid−base pair should be available at the catalyst surface to have an active material. These observations also suggest that novel catalyst materials can be synthesized by modifying the surface composition of basic oxide materials. This can be done by the addition of promotor elements.

Acknowledgment. This work was supported by the National Research School Combination Catalysis (NRSCC) and a NWO-CW VICI grant. We would like to thank P. Bazin (University of Caen, France) for his help with the CO_2 and methanol probing experiments. We also thank A. Mens (Utrecht University) for performing XPS and N_2 physisorption and V. Koot for temperature-programmed desorption. B.M.W. also acknowledges the Dutch Science Foundation (NWO-CW) for a Van Gogh grant for the exchange with the University of Caen. The authors thank one of the referees for the constructive criticism on the acid−base properties of the materials under investigation.

References and Notes

(1) *Guide to Cleaner Technologies: Alternatives to Chlorinated Solvents for Cleaning and Degreasing*; EPA/625/R-93/016; U. S. Environmental Protection Agency; U. S. Government Printing Office: Washington, DC, February 1994.

(2) Erb, J. *Environ. Prog.* **1993**, *12*, 243.

(3) Koper, O.; Li, Y. X.; Klabunde, K. J. *Chem. Mater.* **1993**, *5*, 500.

(4) Hooker, P. D.; Klabunde, K. J. *Chem. Mater.* **1994**, *6*, 1243.

(5) Klabunde, K. J.; Khaleel, A.; Park, D. *High Temp. Mater. Sci.* **1995**, *33*, 99.

(6) Koper, O. B.; Wovchko, E. A.; Glass, J. A.; Yates, J. T.; Klabunde, K. J. *Langmuir* **1995**, *11*, 2054.

(7) Klabunde, K. J.; Stark, J.; Koper, O.; Mohs, C.; Park, D. G.; Decker, S.; Jiang, Y.; Lagadic, I.; Zhang, D. *J. Phys. Chem.* **1996**, *100*, 12142.

(8) Koper, O.; Lagadic, I.; Klabunde, K. J. *Chem. Mater.* **1997**, *9*, 838.

(9) Chien, Y. C.; Wang, H. P.; Yang, Y. W. *Environ. Sci. Technol.* **2001**, *35*, 3259.

(10) Chien, Y. C.; Wang, H. P. *J. Electron Spectrosc. Relat. Phenom.* **2005**, *144*, 315.

(11) Tamai, T.; Inazu, K.; Aika, K. *Chem. Lett.* **2003**, *32*, 436.

(12) Tamai, T.; Inazu, K.; Aika, K. *Bull. Chem. Soc. Jpn.* **2004**, *77*, 1239.

(13) Liu, G. H.; Wang, J. L.; Zhu, Y. F.; Zhang, X. R. *Phys. Chem. Chem. Phys.* **2004**, *6*, 985.

(14) Liu, G. H.; Zhu, Y. F.; Zhang, X. R.; Xu, B. Q. *Anal. Chem.* **2002**, *74*, 6279.

(15) Weckhuysen, B. M.; Mestl, G.; Rosynek, M. P.; Krawietz, T. R.; Haw, J. F.; Lunsford, J. H. *J. Phys. Chem. B* **1998**, *102*, 3773.

(16) Weckhuysen, B. M.; Rosynek, M. P.; Lunsford, J. H. *Phys. Chem. Chem. Phys.* **1999**, *1*, 3157.

(17) Van der Avert, P.; Weckhuysen, B. M. *Phys. Chem. Chem. Phys.* **2004**, *6*, 5256.

(18) Van der Avert, P.; Weckhuysen, B. M. *Angew. Chem., Int. Ed.* **2002**, *41*, 4730.

(19) Van der Avert, P.; Podkolzin, S. G.; Manoilova, O. V.; De Winne, H.; Weckhuysen, B. M. *Chem.—Eur. J.* **2004**, *10*, 1.

(20) Podkolzin, S. G.; Manoilova, O. V.; Weckhuysen, B. M. *J. Phys. Chem. B* **2005**, *109*, 11634.

(21) Manoilova, O. V.; Podkolzin, S. G.; Tope, B.; Lercher, J.; Stangland, E. E.; Goupil, J. M.; Weckhuysen, B. M. *J. Phys. Chem. B* **2004**, *108*, 15770.

(22) Au, C. T.; He, H.; Lai, S. Y.; Ng, C. F. *Appl. Catal., A* **1997**, *159*, 133.

(23) Schweizer, A. E.; Jones, M. E.; Hickman, D. A. U. S. Patent 6,-452,058 B1, 2002.

(24) Brixner, L. H.; Moore, E. P. *Acta Crystallogr.* **1983**, *C39*, 1316.

(25) Morosin, B. *J. Chem. Phys.* **1968**, *49*, 3007.

(26) Attfield, J. P.; Ferey, G. *J. Solid State Chem.* **1989**, *82*, 132.

(27) Binet, C.; Daturi, M.; Lavalley, J. C. *Catal. Today* **1999**, *50*, 207.

(28) Lavalley, J. C. *Catal. Today* **1996**, *27*, 377.

(29) Urban, M. W. *Vibrational Spectroscopy of Molecules and Macromolecules on Surfaces*; John Wiley and Sons, Ltd.: Chichester, 1994.

(30) Skylarenko, Y. S.; Skylarenko, I. S.; Chubukova, T. M. *Zh. Anal. Khim.* **1961**, *16*, 417.

(31) Badri, A.; Binet, C.; Lavalley, J. C. *J. Chem. Soc., Faraday Trans.* **1997**, *93*, 2121.

(32) Binet, C.; Daturi, M. *Catal. Today* **2001**, *70*, 155.